AFRL-RY-WP-TP-2010-1245

EXTRACTION OF SEMICONDUCTOR MICROCHIP DIFFERENTIAL GAIN BY USE OF OPTICALLY PUMPED SEMICONDUCTOR LASER (POSTPRINT)

Jörg Hader and Jerome V. Moloney

Nonlinear Control Strategies

Matthew Walton, Nathan Terry, and Robert Bedford

Electro Optic Components Branch
Aerospace Components and Subsystems Technology Division

SEPTEMBER 2009

AIR FORCE RESEARCH LABORATORY
SENSORS DIRECTORATE
WRIGHT-PATTERSON AIR FORCE BASE, OH 45433-7320
AIR FORCE MATERIEL COMMAND
UNITED STATES AIR FORCE

REPORT DOCUMENTATION PAGE

Form Approved
OMB No. 0704-0188

1. REPORT DATE *(DD-MM-YY)*	2. REPORT TYPE	3. DATES COVERED *(From - To)*
September 2009	Journal Article Postprint	01 January 2009 – 01 September 2009

4. TITLE AND SUBTITLE
EXTRACTION OF SEMICONDUCTOR MICROCHIP DIFFERENTIAL GAIN BY USE OF OPTICALLY PUMPED SEMICONDUCTOR LASER (POSTPRINT)

5a. CONTRACT NUMBER
In-house

5b. GRANT NUMBER

5c. PROGRAM ELEMENT NUMBER
62204F

6. AUTHOR(S)
Jörg Hader and Jerome V. Moloney (Nonlinear Control Strategies)
Matthew Walton, Nathan Terry, and Robert Bedford (AFRL/RYDP)

5d. PROJECT NUMBER
2002

5e. TASK NUMBER
IH

5f. WORK UNIT NUMBER
2002IH0E

7. PERFORMING ORGANIZATION NAME(S) AND ADDRESS(ES)

Nonlinear Control Strategies
Tucson, AZ

Electro Optic Components Branch (AFRL/RYDP)
Aerospace Components and Subsystems
Technology Division
Air Force Research Laboratory, Sensors Directorate
Wright-Patterson Air Force Base, OH 45433-7320
Air Force Materiel Command, United States Air Force

8. PERFORMING ORGANIZATION REPORT NUMBER
AFRL-RY-WP-TP-2010-1245

9. SPONSORING/MONITORING AGENCY NAME(S) AND ADDRESS(ES)
Air Force Research Laboratory
Sensors Directorate
Wright-Patterson Air Force Base, OH 45433-7320
Air Force Materiel Command
United States Air Force

10. SPONSORING/MONITORING AGENCY ACRONYM(S)
AFRL/RYDP

11. SPONSORING/MONITORING AGENCY REPORT NUMBER(S)
AFRL-RY-WP-TP-2010-1245

12. DISTRIBUTION/AVAILABILITY STATEMENT
Approved for public release; distribution unlimited.

13. SUPPLEMENTARY NOTES
Journal article published in *Applied Physics Letters*, Vol. 95, 2009. PAO Case Number: 88ABW-09-2594; Clearance Date: 09 Jun 2009. Paper contains color.

14. ABSTRACT
The small-signal modulation response of a vertical external cavity surface emitting laser is analyzed to determine its resonance frequency in relation to photon density, allowing nondestructive extraction of characteristic parameters of chips, such as internal loss and differential gain.

15. SUBJECT TERMS
lasers, semiconductor

16. SECURITY CLASSIFICATION OF:			17. LIMITATION OF ABSTRACT:	18. NUMBER OF PAGES	19a. NAME OF RESPONSIBLE PERSON (Monitor)
a. REPORT	b. ABSTRACT	c. THIS PAGE			Robert G. Bedford
Unclassified	Unclassified	Unclassified	SAR	10	19b. TELEPHONE NUMBER *(Include Area Code)* N/A

Standard Form 298 (Rev. 8-98)
Prescribed by ANSI Std. Z39-18

Extraction of semiconductor microchip differential gain by use of optically pumped semiconductor laser

Matthew Walton,[a] Nathan Terry, Jorg Hader,[b] Jerome Moloney,[b] and Robert Bedford
Air Force Research Laboratory Sensors Directorate, Wright-Patterson AFB, Ohio 45433-7321, USA

(Received 12 June 2009; accepted 15 August 2009; published online 14 September 2009)

The small-signal modulation response of a vertical external cavity surface emitting laser is analyzed to determine its resonance frequency in relation to photon density, allowing nondestructive extraction of characteristic parameters of chips, such as internal loss and differential gain. © *2009 American Institute of Physics*. [doi:10.1063/1.3222899]

In recent years, the vertical external cavity surface emitting laser (VECSEL)[1–4] has received considerable attention. In the past decade, VECSELs have been investigated for their high power, high efficiency, ability to operate in continuous wave mode, and diffraction-limited beam quality. Employing an "open-cavity" architecture allows the use of intracavity elements such as saturable absorbers and nonlinear crystals.[2,3] Laser dynamics are dramatically affected by the large cavity damping, contributing to low noise floor in VECSELs, indicating potential uses in low-frequency rf sources.[5] Direct source applications most often necessitate digital or analog modulation, e.g., free-space communication or three-dimensional laser RADAR imaging. In some cases, pulsed or mode-locked lasers are suitable, but in others, small- and large-signal modulation is required for flexible signal encoding.[6] While large-signal VECSEL modulation has been studied previously,[4] in this letter, we report an investigation of the small-signal modulation of VECSELs operating between the class A and class B regimes.

Studying the small-signal regime of VECSEL operation has several advantages. First, the simplifications to the full rate equations allow us to more tenably study relations between the photon densities and the carrier density in both the wells and barriers. Second, using the small-signal approximation, the parameters of the coupled equations of a three level system may be extracted by fitting the model to experimental data. Finally, this analysis of VECSELs allows the nondestructive characterization of the internal loss and the differential gain, a definite advantage if these devices are to be incorporated into communications or imaging systems.

The cavity we study is comprised of an epitaxially grown mirror/active region combination and an external curved mirror supporting a stable mode. The active region is composed of a 14 strained quantum-well InGaAs resonant periodic gain region with strain compensating layers designed to operate at approximately 976 nm at 20 °C. The active region is heterogeneously grown with a distributed Bragg reflector composing one mirror of the resonator. Fabrication entails solder bonding the chip to a diamond heat spreader, removing the substrate, and applying a low-reflectance single-layer dielectric coating onto the surface, significantly reducing both pump and lasing reflections from the semiconductor/air interface. Details of this structure and its cw performance can be found elsewhere.[7]

A 200 mm radius of curvature output coupler is placed 3 cm from the microchip, which results in a photon lifetime regime of interest. The cavity is allowed to run in multiple transverse and longitudinal modes with no intracavity filtering elements. The VECSEL chip is pumped with two 808 nm lasers. First, a high-power fiber-coupled laser bar imaged onto the semiconductor surface at an angle of approximately 40° results in a pump ellipse with a minor axis of 200 μm, herein referred to as "bias pump." A second lower power ridge laser is biased above threshold and is sinusoidally modulated with an amplitude of approximately 18 μW. This second ac pump is imaged onto the chip surface and overlaps an area slightly smaller than the bias pump to create the small-signal modulation. The electrical input to the ac pump is adjusted to maintain a constant output optical amplitude independent of modulation frequency, thus explicitly isolating the response of the VECSEL. The combination of these two pumps allows for biasing the VECSEL above threshold and modulating small amplitudes above this bias point, and is not dissimilar to direct-drive modulation of electrically injected lasers.[8] The bias power out of the cavity is maintained at 1 W or less to minimize thermal loading, which is ignored in the model.

The low reflectance dielectric coating allows us to neglect etalon effects in the chip. If we also ignore the weak filtering due to the resonant periodic gain and position the spectral influence of the distributed Bragg reflector, we may analyze the low frequency laser response using coupled differential equations. This chip is barrier pumped, therefore we must consider both well and barrier densities, not unlike that of step confinement heterostructure (SCH) electrically injected lasers.

$$\dot{N}_w = \frac{P_i \Omega_w}{V_w \hbar \omega_p} - R_w - \frac{N_w}{\tau_{bw}} + \frac{V_b}{V_w}\frac{N_b}{\tau_{wb}} - v_g \Gamma_r g_w N_p, \tag{1}$$

$$\dot{N}_b = \frac{P_i \Omega_b}{V_b \hbar \omega_p} - R_b + \frac{V_w}{V_b}\frac{N_w}{\tau_{bw}} - \frac{N_b}{\tau_{wb}}, \tag{2}$$

$$\dot{N}_p = -\frac{N_p}{\tau_p} + v_g \Gamma_r \Gamma g_w N_p + \beta_{sp} \Gamma B_w N_w^2. \tag{3}$$

In the above equations, N_w, N_b, and N_p represent the well, barrier, and photon densities, respectively, while P_i rep-

[a]Electronic mail: matthew.walton@wpafb.af.mil.
[b]Nonlinear Control Strategies, Tucson, AZ, USA.

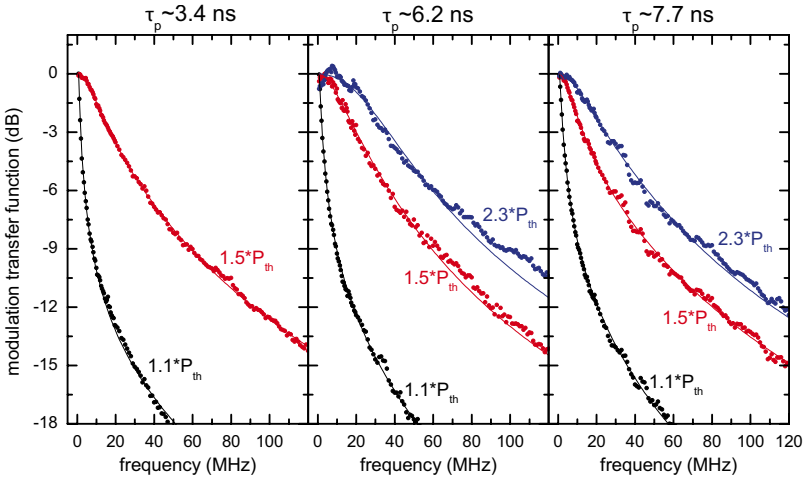

FIG. 1. (Color online) Small signal VECSEL modulation for various photon lifetimes. The points indicate experimental data, while the lines represent our fit using the three-pole MTF.

resents the incident pump power at frequency ω_p, and is absorbed into the well and barrier volumes (V_w and V_b) with efficiency of Ω_w and Ω_b. R_w and R_b represent the typical nonradiative recombination, spontaneous emission, and Auger recombination processes for the wells and barriers (denoted by subscripts) and are functions of their respective carrier densities, N_w and N_b. B_w identifies the spontaneous emission coefficient explicitly. The coupling lifetimes between the wells and barriers are identified as τ_{wb} and τ_{bw}, similar to those of a SCH.[9,10] The group velocity within the semiconductor active region is given by v_g, and the quantum well material gain is g_w. Resonant gain enhancement is Γ_r.[11] The three-dimensional mode overlap with the gain region is Γ, and the fraction of the photons captured by the VECSEL cavity is β_{sp}. Finally, the photon lifetime (τ_p) is used here as a slight modification to the more typical version,

$$\frac{1}{\tau_p} = \frac{1}{2}\frac{cv_g}{v_g L_p + cL_a}\left[\ln\left(\frac{1}{R_1 R_2}\right) + \ln\left(\frac{1}{S^2}\right)\right]. \tag{4}$$

In Eq. (4), L_a is the thickness of the semiconductor active region, L_p is the length of the passive cavity, c is the vacuum speed of light, R_1 is the reflectivity of the distributed Bragg reflector, R_2 is the reflectivity of the out-coupler, and S^2 accounts for the power lost due to scattering at the surface of the chip. The scattering can be experimentally determined through analysis of the slope efficiency,

$$\frac{\partial P_o}{\partial P_i} = \frac{\ln\left(\frac{1}{R_2}\right)}{\ln\left(\frac{1}{R_1 R_2}\right) + \ln\left(\frac{1}{S^2}\right)}\Gamma_T \Delta_p \Omega, \tag{5}$$

where P_o indicates bias output, Γ_T is the transverse field confinement within the gain region, Δ_p is the quantum defect, and Ω is the fraction of light absorbed by the barriers and wells in the active region ($\Omega \equiv \Omega_w + \Omega_b$). For this particular chip, the scatter S is found to be 0.992; the total absorption is about 70%.

To determine the small-signal response, the VECSEL output is coupled to a multimode fiber which is incident on a 26 GHz photodetector ac coupled to a 2 GHz rf spectrum analyzer. To develop a modulation transfer function (MTF), we sweep the modulated laser across the microwave spectrum, recording each detected rf signal from the spectrum analyzer. In much the same way as modulation in lasers, both well and barrier carriers are allowed to oscillate with the pump, and their response is damped by the carrier and photon lifetimes.

We are able to change cavity parameters and characterize the operating properties of the chip. For example, photon lifetime may be varied simply by changing the outcoupling mirror, resulting in a change to the photon lifetime as governed by Eq. (4). Reflectivities of approximately 96%, 98%, and 99% are used to adjust the photon lifetime to 3.4, 6.2, and 7.7 ns, respectively. Particular care is taken to avoid transverse mode hopping, which at higher pump powers causes fluctuations in output power.

The gain region of the VECSEL is a very small fraction of the cavity, resulting in a Γ on the order of 10^{-6}. This fact allows us to neglect the relative contribution of the direct well pumping, therefore the output of the VECSEL modulates as a function of frequency, ω, according to the three pole formula

$$H(\omega) \approx \frac{1}{1 + i\tau_{wb}\omega}\frac{\omega_r^2}{\omega_r^2 - \omega^2 + i\gamma\omega}. \tag{6}$$

The angular frequency is ω_r, γ is the associated damping, and τ_{wb} is the barrier to well carrier lifetime,[12] which dominates over direct nonradiative recombination in the barriers R_b.

Figure 1 shows the MTF for particular pump powers (in units of threshold) against modulation frequency for 3.4, 6.2, and 7.7 ns photon lifetimes. Data are taken for modulation frequencies up to 120 MHz. The data, indicated by the points in Fig. 1 are fitted with Eq. (6), and plotted as solid lines. Resonance frequency, damping, and differential gain are extracted from the data and reported in Table I for output powers of 300 mW. The square of angular resonance frequency, w_r^2 can be approximated by[12]

TABLE I. Resonance frequencies (ω_r), damping (γ), and differential gain ($\partial g/\partial N_w|_{\langle N_w \rangle}$) for various photon lifetimes at P_o=300 mW.

τ_p (ns)	3.4	6.2	7.7
$\omega_r/2\pi$ (MHz)	21.3	23.3	29.8
$\gamma/2\pi$ (MHz)	51.7	53.8	71.1
$\partial g/\partial N_w\|_{\langle N_w \rangle}$ (cm^2)	8.5×10^{-16}	8.8×10^{-16}	1.2×10^{-15}

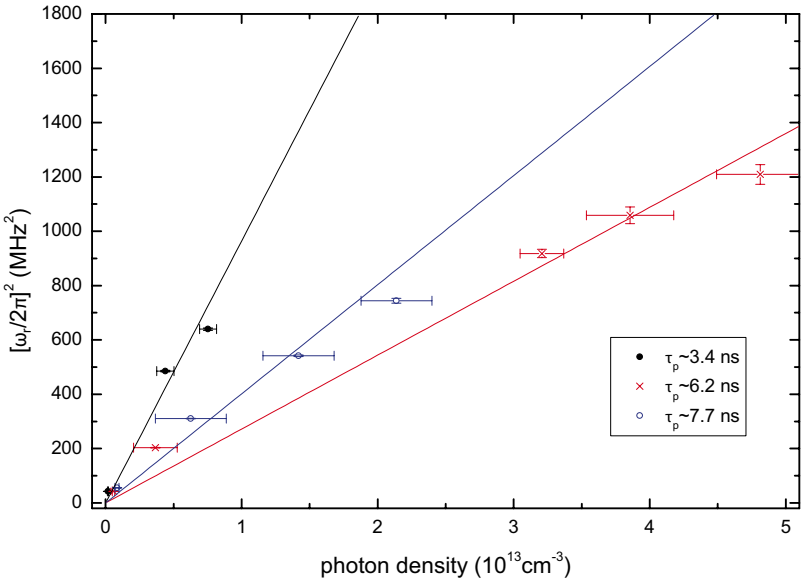

FIG. 2. (Color online) Resonant frequency squared as a function of calculated photon density. Linear fits to this data reveal the differential gain at that photon lifetime.

$$\omega_r^2 \approx \left.\frac{v_g}{\tau_p}\frac{\partial g}{\partial N_w}\right|_{\langle N_w\rangle} N_p, \tag{7}$$

where the differential gain is expressed as $(\partial g/\partial N_w|_{\langle N_w\rangle})$. It is also worth noting the existence of a resonance peak for the case of τ_p=6.2 ns, but this peak is not evident in the MTF when τ_p=7.7 ns. When the photon lifetime exceeds the carrier lifetime, the response is overdamped, and the relaxation oscillation is absent. An analogous case in semiconductor lasers is found in the quantum cascade laser, where the carrier lifetime is reduced to picoseconds, on the same order of magnitude as the photon lifetime.[13] In the case of the VECSEL reported, the photon lifetime is on the order of the carrier lifetime, and therefore as we increase the photon lifetime, the relaxation oscillation is extinguished.

The resonance frequencies in Table I increase with larger photon lifetimes, which appears contrary to Eq. (7), until one considers that the P_o relation to N_p itself is a function of photon lifetime. This is why these results do not directly show the inverse relation as indicated by Eq. (7). Without nonmirror cavity loss, the output power is proportional to N_p/τ_p, canceling the τ_p in Eq. (7). The more general case must also consider the fraction of out-coupling mirror loss relative to the total loss [explicitly defined in Eq. (5)]. This relationship between power and photon density is accounted for in Fig. 2.

Equation (7) shows that the square of the resonance frequency is inversely proportional to photon lifetime and also increases for higher photon densities. Measuring the MTF at several output powers for various photon lifetimes, we plot the relation of $(\omega_r/2\pi)^2$ relative to the photon density. Figure 2 shows the square of the resonance frequency with respect to the photon density for three photon lifetimes. The slope of the fit is proportional to the differential gain.

This experiment characterizes the small-signal modulation of a VECSEL to gain insight into a use of semiconductor lasers that has been largely overlooked. The ability to nondestructively adjust the photon lifetime allows for characterization of semiconductor parameters such as differential gain, and device parameters such as scattering loss. Despite neglecting direct well-pumping, we show the three-pole model describes the behavior of the VECSEL cavity which satisfies particular approximations. With sufficient data, one may map the gain carrier relation to within a constant and tailor models to appropriately predict actual device performance. Thus, the characterization of VECESLs operating in the small-signal regime is an important step in using VECESLs for low-frequency imaging and communication systems.

We thank V. Kovanis for fruitful discussions. This work is supported in part by AFOSR laboratory task Grant No. 08RY08COR.

[1]M. Kuznetsov, F. Hakimi, R. Sprague, and A. Mooradian, IEEE J. Sel. Top. Quantum Electron. **5**, 561 (1999).
[2]A. Wójcik-Jedlińska, J. Muszalski, and M. Bugajski, J. Phys.: Conf. Ser. **146**, 012031 (2009).
[3]Y. Morozov, T. Leinonen, M. Morozov, S. Ranta, M. Saarinen, V. Popov, and M. Pessa, New J. Phys. **10**, 063028 (2008).
[4]S. Chatterjee, W. Diehl, S. Horst, K. Hantke, W. W. Stolz, A. Thranhardt, S. W. Koch, P. Brick, M. Furitsch, S. Illek, I. Pietzonka, J. Luft, and W. W. Ruhle, *Technical Digest Series* (Optical Society of America, Washington, D.C., 2007), p. 4431387.
[5]G. Baili, M. Alouini, T. Malherbe, D. Dolfi, J.-P. Huignard, T. M. Jean Chazelas, I. Sagnes, and F. Bretenaker, Opt. Express **16**, 10091 (2008).
[6]R. Häring, R. Paschotta, A. Aschwanden, E. Gini, F. Morier-Genoud, and U. Keller, IEEE J. Quantum Electron. **2**, 1268 (2002).
[7]L. Fan, M. Fallahi, J. Hader, A. R. Zakharian, M. Kolesik, J. V. Moloney, T. Qiu, A. Schülzgen, N. Peyghambarian, W. Stolz, S. W. Koch, and J. T. Murray, Appl. Phys. Lett. **86**, 211116 (2005).
[8]S. D. Offsey, W. J. Schaff, L. F. Lester, L. F. Eastman, and S. K. McKernan, IEEE J. Quantum Electron. **27**, 1455 (1991).
[9]L. Davis, Y. L. Lam, Y. C. Chen, J. Singh, and P. Bhattacharya, IEEE J. Quantum Electron. **30**, 2560 (1994).
[10]A. R. Zakharian, J. Hader, J. V. Moloney, S. W. Koch, P. Brick, and S. Lutgen, Appl. Phys. Lett. **83**, 1313 (2003).
[11]S. Corzine, R. Geels, J. Scott, R. H. Yan, and L. Coldren, IEEE J. Quantum Electron. **25**, 1513 (1989).
[12]L. Coldren and S. Corzine, *Diode Lasers and Photonic Integrated Circuits* (Wiley, New York, 1995).
[13]F. Rana and R. J. Ram, Phys. Rev. B **65**, 125313 (2002).